

# OBSERVATIONAL LIMITS ON QUANTUM GEOMETRY EFFECTS

TOMASZ J. KONOPKA AND SETH A. MAJOR

ABSTRACT. Using a form of modified dispersion relations derived in the context of quantum geometry, we investigate limits set by current observations on potential corrections to Lorentz invariance. We use a phenomenological model in which there are separate parameters for photons, leptons, and hadrons. Constraints on these parameters are derived using thresholds for the processes of photon stability, photon absorption, vacuum Čerenkov radiation, pion stability, and the GZK cutoff. Although the allowed region in parameter space is tightly constrained, non-vanishing corrections to Lorentz symmetry due to quantum geometry are consistent with current astrophysical observations.

## 1. INTRODUCTION

The quantum description of gravitation is arguably the largest gap in our understanding of fundamental physics. In the last decade, a number of lines of research have offered new insights into the theory which will supersede quantum theory and general relativity. For instance, several approaches predict that space is fundamentally discrete. In one approach, eigenvalues of geometric observables have discrete spectra (see e.g. [1] for a review). While it may not be surprising that the quantization of curved space yields quantized geometry, it is surprising that present day astronomical observations *already* limit the extent of quantum geometry effects [2–14].

These quantum geometry effects arise from an imprint of discrete underlying space on propagating modes. Particles with ultra-high energies interact with structure on the smallest possible scales resulting in corrections to Lorentz symmetry. Observations on the TeV scale offer an opportunity to test the extent of these quantum geometry induced Lorentz symmetry corrections.

Lorentz invariance may be the most tested symmetry in Nature. Given the wealth of evidence in its support, it may seem obtuse to suggest that there may be corrections. However, there are reasons to believe that this may not be an exact symmetry not the least of which is the fact that any test of Lorentz invariance (necessarily at finite energy) leaves an infinite parameter space untested. Due to the non-compact nature of the Lorentz group, exact Lorentz symmetry is untestable. There are other reasons to suspect exact Lorentz invariance at all energy scales. For instance, ultraviolet divergences in quantum field theory point to new physics at high energies. Despite these suggestions, only recently has work in quantum gravity yielded concrete proposals on how the symmetry might be modified [2, 3, 15–18].

In this paper we explore the consequences of modified dispersion relations which are motivated by a study of semiclassical states in loop quantum gravity by Alfaro, Morales-Técotl, and Urrutia [16, 17]. We study a model in which the usual

---

*Date:* January 2002.

dispersion relation of special relativity,  $E^2 = p^2 + m^2$ , is modified by leading order quantum geometry corrections of the form  $\kappa \ell_p p^3$ . By the semiclassical analysis, the parameter  $\kappa$  is expected to be of order unity. It determines the extent of the corrections to Lorentz symmetry while the Planck length,  $\ell_p$ , sets the scale of the effects. Due to the sensitivity of process thresholds, the modifications of particle dispersion relations are already tested by current astronomical observations.

What is more spectacular than merely limiting the possible extent of corrections to Lorentz symmetry is the proposal [19] that this framework may be robust enough to elegantly explain three incongruities, or paradoxes, between standard model predictions and observational results: (i) Cosmic rays are expected interact with the cosmic microwave background (CMB) producing pions and introducing an upper limit on the observed energy of particles of cosmological origin. Known as the GZK cutoff [20, 21] this upper limit has not been observed. About twenty events at significantly higher energies have been reported [22, 23]. Modified dispersion relations can raise the GZK cutoff [5]. (ii) Ultra high energy photons of cosmic origin are also expected to interact with infra red background radiation. According to some estimates for the background flux, photons of energy 10 TeV or more should not be seen due to background induced pair production [24]. However, higher energy events have been reported [25, 26]. Corrections to Lorentz invariance provides one explanation for this apparent paradox [6]. (iii) Observations of longitudinal development in extensive air showers of high energy hadronic particles are apparently inconsistent with predictions [27]. As proposed in Ref. [27], one possible explanation is that high energy neutral pions become stable. This may also be explained using modified dispersion relations [19].

We calculate thresholds for processes involving photons, leptons and hadrons and, with observational limits, constrain the values for the  $\kappa$  parameters thereby confining the extent of quantum geometry corrections. In more detail, in the next section we summarize the results of Alfaro *et. al.* [16, 17]. Specifying only general properties of a semiclassical state, such as flatness above a characteristic scale  $L$ , the authors find that, in an analysis of particle propagation, photon [17] and neutrino [16] dispersion relations are modified. In Section 3 we give a brief overview of threshold calculations before turning to a number of processes including: photon stability, photon non-absorption, vacuum Čerenkov radiation for electrons and protons, proton non-absorption, and pion stability. We calculate constraints from the threshold calculations to investigate whether it is possible that observed effects may be accounted for by Lorentz symmetry corrections. In 3.2 we show that asymmetric momentum partitioning, first noticed by Liberati, Jacobson, and Mattingly [13], dramatically affects the constraints on the dispersion relation modifications. The results of Section 3 are summarized in Table 1. Finally in Section 4, we apply the constraints together with current observations to limit the extent of potential Lorentz symmetry corrections. We summarize the constraints in the final section and in Figures 2 and 3. We find that present day observations tightly constrain – but still leave open – the possibility of Lorentz symmetry corrections of this form.

Particularly close to the present work is the paper by Jacobson, Liberati, and Mattingly [13] in which many of these results were summarized. For the most part the present work agrees with this paper where the subject overlaps, although this work also includes new threshold calculations and constraints for proton vacuum Čerenkov radiation, the GZK threshold, and pion stability.

## 2. MODIFIED DISPERSION RELATIONS

To determine the action of the Maxwell Hamiltonian operator on quantum geometry Alfaro *et. al.* specify only very general conditions for the semiclassical state. The idea is to work with a class of states which satisfy the following conditions: (i) The state is “peaked” on flat and continuous geometry when probed on length scales larger than a characteristic scale  $L$ ,  $L \gg \ell_p$ . (ii) On length scales larger than the characteristic length the state is “peaked” on the classical Maxwell  $U(1)$  connection. (iii) The expectation values of operators are assumed to be well-defined. In addition it is assumed that the geometric corrections to the expectations values may be expanded in powers of the ratio of the physical length scales,  $L$  and  $\ell_p$ .

States peaked on geometry and the geometric connection are the natural expectation for semiclassical or coherent states which model flat space. The work of Alfaro *et. al.* is a forerunner for the detailed analysis of semiclassical states. As the specification of semiclassical states becomes more precise, and work is well under way [29–35], we can expect to check these initial results.

Expanding the quantum Maxwell Hamiltonian on their states Alfaro *et. al.* find that for massive neutrinos the particle dispersion relations are modified with [16]

$$E_{\pm}^2 = p^2 + m^2 + (\kappa \pm \beta)\ell_p p^3 \quad (1)$$

where  $p$  is the magnitude of the 3-momentum,  $\kappa$  and  $\beta$  are of order unity and  $\beta$  is helicity-dependent. The result is computed for a superposition of helicity eigenstates.

For photons the authors find that the quantum geometry effects are given, to leading order in  $\ell_p k$ , by [17]

$$E_{\gamma}^2 = k^2 + 2\alpha k^{4+2\Upsilon} \ell_p^{2+2\Upsilon} \pm 4\beta \ell_p k^3 \quad (2)$$

where  $\Upsilon$  parameterizes the scaling of the semiclassical state expectation value with respect to the gravitational connection. As before, the parameters  $\alpha$  and  $\beta$  are of order unity with  $\beta$  parameterizing helicity dependent corrections.<sup>1</sup> For the purposes of exploring the leading order helicity-independent effects in this model of quantum geometry, we take  $\Upsilon = -1/2$  and  $\beta = 0$ . Helicity effects have been investigated in Ref. [36] and may be treated using similar methods used in the present work.

To place all the particles we consider on the same footing we take a phenomenological approach in which the modification to the usual dispersion is parameterized by a parameter  $\kappa_a$  for particle species  $a$ . Thus, the effect is simply modeled by the modified dispersion relation

$$E_a^2 = p_a^2 + m_a^2 + \kappa_a \ell_p p_a^3. \quad (3)$$

In this equation  $p$  is the magnitude of the particle 3-momentum, a quantity greater than 0.<sup>2</sup> For each particle species, the parameter  $\kappa_a$  is, from the semiclassical analysis, expected to be of order 1 and can take either sign. Of particular interest to determine whether positive  $\kappa_a$ 's are allowed for massive particles. In this case, massive particles would be able to propagate faster than the low energy speed of light,  $c$ , which has interesting repercussions for causality. Alternately, for either sign

<sup>1</sup>The specification for the class of semiclassical states is more general in [17] than in [16]. With the same specification as the photon case, the neutrino dispersion relation (1) would have the same form as (2) [28].

<sup>2</sup>Since Eq. (3) is in terms of the magnitude, the relation is invariant under time-reversal. The modification could also be viewed as a  $\kappa \ell_p p^2 E$  term.

of  $\kappa_a$ , the particles might be able to propagate faster than high energy photons as long as  $\kappa_a > \kappa_\gamma$ .

In terms of bookkeeping, we use  $\ell_p := \sqrt{4\pi\hbar G/c^3}$  throughout. We set the low energy speed of light to one (“c is c is 1”) and  $\hbar$  to one. The scale of the model becomes  $\ell_p \sim 3 \times 10^{-28} \text{ eV}^{-1}$ . The effects of the correction terms become significant when the correction term is of the same magnitude as the mass term, i.e. when  $p_{crit} \approx (m^2/\ell_p)^{1/3} \sim 10^{13}, 10^{14}$ , and  $10^{15} \text{ eV}$  for electrons, pions, and protons, respectively.<sup>3</sup>

The dispersion relation of Eq. (3) is not valid for all momenta. Since the class of semiclassical states identified by Alfaro *et. al.* only reproduces flat geometry on scales larger than  $L$ , we can only use the dispersion relation within this approximation; particles we investigate cannot have wavelengths shorter than  $L$ . Thus, the momenta are restricted by  $p_a \ll 1/\ell_p$ . We remain well within this restriction with  $\ell_p p_a < 10^{-8}$ .

We call the modification of the dispersion relations “quantum geometry effects” since the background quantum geometry only provides the scale on which new non-linear terms enter the equations of the motion. In addition the quantum geometry of the semiclassical state enjoys no reaction due to propagating modes on the geometry. It is clear that beyond the realm of the semiclassical model reaction of the particle on the geometry must be taken into account and we should expect new behavior.

Throughout this discussion we assume that the momenta, energies, and lengths are compared in one inertial frame. Indeed, if Lorentz symmetry is inexact then there is presumably a preferred frame (however see, for instance, Refs. [39–41] for modifications of Lorentz symmetry which do not select a preferred frame). For the purposes of this phenomenological study, we work in the preferred reference frame in which the cosmic microwave background radiation is isotropic.

Within the context of perturbative quantum field theory it is well known that modified dispersion relations can yield causality violations and breakdowns in perturbative quantization (see, for instance, [42]). Since we investigate particles for which the correction terms play a significant role, these issues are important. However, in the following we work in a single inertial frame and do not have the transformations between inertial frames in this new context. So we leave investigations of these issues to future work. It would be particularly interesting to precisely characterize modified dispersion relations which are consistent within the low energy perturbative framework.

### 3. PARTICLE PROCESSES

On account of the modification in the dispersion relation of Eq. (3) quantum geometry effects are potentially observable. This is due to the sensitivity of process thresholds to the correction term for ultra-high energy particles. We outline the framework of the threshold calculations then present the details of each of the processes in turn.

**3.1. Threshold Kinematics.** Suppose we have the 2 particle interaction  $a + b \rightarrow c + d$ . We assume that energy is conserved,  $E_a + E_b = E_c + E_d$ , and 3-momentum

---

<sup>3</sup>Incidentally, this shows why high precision tests of Lorentz invariance such as in Refs. [37] and [38] do not offer strong limits on the  $\kappa$  parameters. The energies are too low. However, if the characteristic length scale of the semiclassical state were fixed at much larger scale - say nuclear - then these high precision tests would offer limits on the analogous parameters of such a model.

is conserved,  $\mathbf{p}_a + \mathbf{p}_b = \mathbf{p}_c + \mathbf{p}_d$ . The only unusual bit is in the modified dispersion relations. Although the modified threshold calculations are a straightforward application of momentum conservation, energy conservation and the modified dispersion relations, the calculations are not without surprises. In fact, even when the outgoing particles have the same mass, it may not be energetically favorable to partition the momentum symmetrically. This asymmetry was, to our knowledge, first observed by Liberati, Jacobson, and Mattingly [13].

We almost exclusively use the leading order approximation of Eq. (3)

$$E \approx p + \frac{m^2}{2p} + \frac{1}{2}\kappa\ell_p p^2. \quad (4)$$

It is clear that this approximation applies for high energy particles only, when  $p \gg m$  so that  $m \ll p \ll 1/\ell_p$ .

The interaction geometry may be strongly affected by the correction term. At ultra-high momenta the correction term dominates and, if the sign of  $\kappa$  is negative then the energy of the outgoing particles may be reduced by including transverse momenta. However in the regimes we consider, using 4-momentum conservation and these modified dispersion relations it is not hard to see that the threshold interaction geometry is what one would expect: the incoming particles' momenta are antiparallel and the outgoing particles' momenta are parallel. Of course, the momenta must be sub-Planckian. We also emphasize that, in these dispersion relations, the  $\kappa$ -parameters are of order one. Since the framework of the semiclassical states requires that the momenta be far below the Planck scale, we employ this interaction geometry throughout the remainder of this paper.

We use the modified dispersion relation Eq. (4) in the conservation of energy. With energy and momentum conservation, we find the kinematic constraint

$$\frac{m_a^2}{2p_a} + \frac{1}{2}\kappa_a\ell_p p_a^2 + \frac{m_b^2}{2p_b} + \frac{1}{2}\kappa_b\ell_p p_b^2 = \frac{m_c^2}{2p_c} + \frac{1}{2}\kappa_c\ell_p p_c^2 + \frac{m_d^2}{2p_d} + \frac{1}{2}\kappa_d\ell_p p_d^2. \quad (5)$$

By momentum conservation  $p_d = p_i - p_c$  with  $p_i := p_a + p_b$  being the available incoming momentum. Thus the right hand side of Eq. (5) may be expressed as a function of  $p_c$  only.

To locate the threshold for one of the incoming particles (typically, the other momenta is known), we wish to find the minimum final energy as a function of the momentum of the outgoing particle  $c$ . This may be accomplished by differentiating Eq. (5) and finding the roots. In the general two-channel case, this is given by

$$0 = -\frac{m_c^2}{2p_c^2} + \kappa_c\ell_p p_c + \frac{m_d^2}{2(p_i - p_c)^2} + \kappa_d\ell_p(p_i - p_c) \quad (6)$$

which is a quintic in  $p_c$ . With the physical root(s) in hand one can return to Eq. (5) to find the threshold momentum. However, in the individual processes there are better methods than attempting to directly solve this quintic. Perhaps the best way to see this is in the case of photon stability. As this case is straightforward and yet gives asymmetric partitioning we present it in its entirety.

**3.2. Photon Stability:**  $\gamma \not\rightarrow e^+ + e^-$ . In special relativity photon decay is forbidden – a simple consequence of the energy and momentum conservation. However, taking quantum geometry effects into account it is energetically favorable for ultra-high energy photons to decay. Recent observations of multi-TeV photons [25, 26, 43] provide potential threshold values for the quantum geometry induced decay.

Applying the threshold framework above, we immediately see that there are considerable simplifications in Eq. (5). In fact, the energy-momentum constraint becomes

$$\kappa_\gamma \ell_p p_\gamma^2 = m_e^2 \left( \frac{1}{p_{e+}} + \frac{1}{p_{e-}} \right) + \kappa_e \ell_p (p_{e+}^2 + p_{e-}^2). \quad (7)$$

Before differentiating, notice that for negative  $\kappa_\gamma$ , the electron  $\kappa$ -parameter must also be negative. This opens up the possibility that a simple  $p_\gamma/2$  partition of incoming momenta may not be energetically favorable.

This is already clear from the modified dispersion relations for negative  $\kappa_a$ . As the momentum of the particle increases the energy increases. However, when the momentum is near  $p_{crit}$  the energy increases less rapidly.<sup>4</sup> This curve strongly affects the nature of threshold calculations: At high momentum the slope of the energy steadily decreases so it becomes energetically favorable to partition the momentum of the outgoing particles asymmetrically. By asymmetrically partitioning momentum one can only slightly increase the energy of the high momentum particle while drastically reducing the energy of the lower momentum particle leading to a lower total energy (for more extensive discussion see Ref. [44]).

With this observation we re-express the outgoing momenta as  $p_{e-} = p_o - \Delta$  and  $p_{e+} = p_o + \Delta$  with  $p_o$  being half the available momentum,  $p_o := p_\gamma/2$ . The asymmetry factor  $\Delta$  can be no larger than  $p_o$ ;  $-p_o < \Delta < p_o$ . The relation Eq. (7) becomes

$$2\kappa_\gamma \ell_p p_o^2 = \frac{m_e^2 p_o}{p_o^2 - \Delta^2} + \kappa_e \ell_p (p_o^2 + \Delta^2). \quad (8)$$

To find the threshold energy, or minimum energy, for this process we minimize this equation. This yields a simple quartic for  $\Delta$  which has two physical roots:  $\Delta_* = 0$  for the symmetric and

$$\Delta_*^2 = p_o^2 \left( 1 - \sqrt{\frac{m_e^2}{-\kappa_e \ell_p p_o^3}} \right) \quad (9)$$

for the asymmetric partitioning, respectively. The second root is only real for negative  $\kappa_e$ . Since the momenta asymmetry is bounded by  $p_o$  there is an upper bound on  $\kappa_e$  for this root:

$$\kappa_e \leq -\frac{m_e^2}{\ell_p p_o^3}. \quad (10)$$

In addition, when the threshold energy is found using asymmetric root another condition is required to ensure that all the momenta are non-negative. This condition is  $\kappa_\gamma > \kappa_e$ .

To find the regions of  $\kappa$ -parameter space where the two roots impose constraints, it is worth returning to Eq. (8). As observed above, if  $\kappa_\gamma$  is negative then  $\kappa_e$  is as well. It is then energetically advantageous to asymmetrically partition the momentum, i.e. to use the non-zero root  $\Delta_*$ . Thus, when both  $\kappa_\gamma < 0$  and the

---

<sup>4</sup>At high momentum, at the limit of the semiclassical approximation, the energy reaches a maximum. Understanding what occurs at these energies requires detailed knowledge of the dynamics in addition to the semiclassical state of quantum gravity.

inequality of (10) is satisfied the asymmetric configuration is applicable. With the two roots and the energy-momentum constraint, the momenta at threshold are

$$p_{\gamma_*} = \left[ \frac{8m_e^2}{(2\kappa_\gamma - \kappa_e)\ell_p} \right]^{1/3} \quad \text{for } \kappa_\gamma \geq 0$$

and

$$p_{\gamma_*} = \left[ \frac{-8\kappa_e m_e^2}{(\kappa_\gamma - \kappa_e)^2 \ell_p} \right]^{1/3} \quad \text{for } \kappa_e < \kappa_\gamma < 0$$
(11)

where the two thresholds are valid in the regions identified by the inequalities.

Given a threshold value  $p_{\gamma_*}$  for the process, these equations give relationships between  $\kappa_e$  and  $\kappa_\gamma$ . Since the photon is stable if the incoming energy is less than the threshold energy, we can assign inequalities to the constraints on  $\kappa_e$  and  $\kappa_\gamma$ . Thus, the photon is stable at the threshold  $p_{\gamma_*}$  if

$$\kappa_\gamma - \frac{1}{2}\kappa_e - \frac{4m_e^2}{\ell_p p_{\gamma_*}^3} < 0 \quad \text{for } \kappa_\gamma \geq 0 \quad \text{and}$$

$$(\kappa_\gamma - \kappa_e)^2 + \frac{8m_e^2}{\ell_p p_{\gamma_*}} \kappa_e < 0 \quad \text{for } \kappa_e < \kappa_\gamma < 0.$$
(12)

The regions of applicability of the two constraints are inherited from the momenta thresholds. These constraints, together with the regions of applicability, determine allowed regions in the  $\kappa$  parameter space.

The highest energy observed gamma ray, 50 TeV, originated from the relatively local Crab nebula [43]. Using this energy for  $p_{\gamma_*}$  we plot the constraints of (12) in Fig. (1). The constraint inequalities ensure that the photon does not decay below this threshold. The shading represents regions in  $\kappa_e - \kappa_\gamma$  space which are ruled out by the constraints of (12). The smooth transition from the linear to the quadratic constraints on the  $\kappa$  parameters occurs when  $\kappa_\gamma$  changes sign. The resulting curve forms the upper bound on the allowed region.

There is another process which has a closely related calculation. This is the apparent paradoxical observations of TeV photons from distant sources.

**3.3. Photon non-absorption:**  $\gamma + \gamma_{IR} \not\rightarrow e^+ + e^-$ . Due to the presence of background radiation, high-energy photons are expected to be absorbed in pair creation by the far infra-red (IR) background. For photons originating from distances greater than  $\sim 100$  Mpc, the 0.025 eV background provides a cutoff in the spectrum at  $\sim 10$  TeV. However, recent observations of multi-TeV photons have challenged this expectation [25, 26]. Located at redshift  $\sim 0.03$  the active galactic nuclei Markarian 421 and Markarian 501 have produced flares with multi-TeV photons. Observations have included 17 TeV [25] and 24 TeV [26] events. It has been suggested that the apparent overabundance of high energy photons may be due to corrections to Lorentz invariance along the lines of Eq. (3) [10].

The process kinematics is identical with the case of photon stability of Eq. (8) except the presence of the IR photon. Letting the energy of this low-energy photon be  $\epsilon$ , conservation of momentum for this process becomes  $p_\gamma - \epsilon = p_{e^+} + p_{e^-}$  and equation for photon absorption becomes identical to Eq. (8) with the substitution [13]

$$\kappa_\gamma \rightarrow \kappa'_\gamma := \kappa_\gamma + \frac{4\epsilon}{p_\sigma^2 \ell_p}.$$

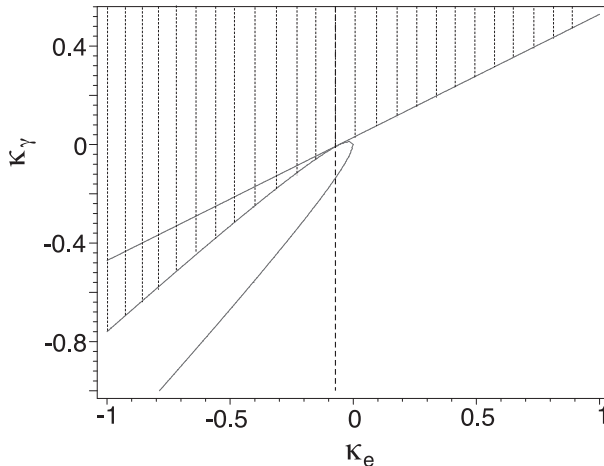


FIGURE 1. Using the thresholds for photon stability and a threshold value of 50 TeV, the two constraints are plotted. The two curves smoothly intersect at the transition from symmetric partitioning, the diagonal line, to asymmetric partitioning, the quadratic function in the third quadrant. The vertical dashed line is the condition of Eq. (10). This identifies the upper branch of the asymmetric constraint as the physical solution. The region ruled out by photon stability up to 50 TeV is indicated with shading.

Thus, the calculation of the threshold is the same as for photon stability and resulting  $\kappa$  inequalities are identical with the substitution  $\kappa_\gamma \rightarrow \kappa'_\gamma$ . Because of the factor of  $p_o$  in the definition of  $\kappa'_\gamma$ , it is not as straightforward to write simple expressions for  $p_{\gamma^*}$ . Our main interest is on the allowed regions in  $\kappa$  parameter space so we are satisfied with the equations which relate  $\kappa_e$  and  $\kappa_\gamma$  for the allowed region. These are presented in Table 1. Plots of the allowed region are similar in form to the ones for photon stability.

**3.4. Pion Stability:**  $\pi \not\rightarrow \gamma + \gamma$ . Within the context of ordinary particle kinematics, the neutral pion has a lifetime of  $8 \times 10^{-17}$  s. As suggested by Amelino-Camelia [19], the modified dispersion relations can have the effect of making ultra-high energy neutral pions stable. This may explain some inconsistencies between observed and expected patterns in cosmic ray showers.

Normally the pion decays because the rest mass can be converted into energy in the form of photons. With the modified dispersion relations, it is possible that, above a threshold energy, it is no longer kinematically possible for the pion to decay.

The threshold calculation is similar to photon stability. Proceeding as before we asymmetrically partition the available momentum for the two photons,  $p_o - \Delta$  and  $p_o + \Delta$ . The resulting energy-momentum constraint is

$$\frac{m_\pi^2}{2p_o} + 4\kappa_\pi \ell_p p_o^2 = 2\kappa_\gamma \ell_p (p_o^2 + \Delta^2). \quad (13)$$

As is clear from this equation the analysis splits into two cases depending on the sign of  $\kappa_\gamma$ . For  $\kappa_\gamma > 0$  the minimization requires symmetric partitioning:  $\Delta_* = 0$ .



Solving Eq. (13) for the threshold momentum we have

$$p_{\pi_*} = \left[ \frac{2m_\pi^2}{(\kappa_\gamma - 2\kappa_\pi)\ell_p} \right]^{1/3} \quad \text{for } \kappa_\gamma > 0 \text{ and } \kappa_\gamma > 2\kappa_\pi. \quad (14)$$

The last inequality ensures that the momentum is positive.

In the second case,  $\kappa_\gamma < 0$ , the symmetric partitioning is in fact the worst choice we could make. Equal photon momenta is the maximum of the outgoing energy. The local minimum for the energy of the outgoing photons is at the maximum possible asymmetry,  $\Delta_* = p_o = p_\pi/2$ , corresponding to the threshold emission of a zero momentum photon. From Eq. (13), the threshold momentum for this process is bounded from below

$$p_{\pi_*} > \left[ \frac{m_\pi^2}{(\kappa_\gamma - \kappa_\pi)\ell_p} \right]^{1/3} \quad \text{for } \kappa_\gamma < 0 \text{ and } \kappa_\gamma > \kappa_\pi. \quad (15)$$

The first inequality for  $\kappa_\gamma$  ensures that the energy remains positive while the last ensures that the threshold momentum is positive.

In an identical manner to the previous calculations, Eq. (14) and (15) yield inequalities among  $\kappa_\pi$  and  $\kappa_\gamma$ . These are summarized in Table 1.

**3.5. Vacuum Čerenkov Radiation:**  $a \rightarrow a + \gamma$ . Čerenkov radiation is observed when a charged particle enters a medium with a speed greater than the phase velocity of electromagnetic waves in the medium. Vacuum Čerenkov radiation in which empty flat space constitutes the medium is normally forbidden by ordinary threshold kinematics. However, Coleman and Glashow suggested that within the context of a variable-speed-of-light theory, vacuum Čerenkov radiation could be induced when a charged particle's speed exceeds the local speed of light [4] (see also [11]). Vacuum Čerenkov radiation (VČR) may also be kinematically allowed by the modified dispersion relations. This is clear even from a glance at a charged particle's speed

$$v_a = \frac{\partial E_a}{\partial p_a} = 1 - \frac{m_a^2}{2p_a^2} + \kappa_a \ell_p p_a \quad (16)$$

where  $a$  is the charged particle.

Since both charged particles and photons have the same functional form of the dispersion relations, there are four possible cases to investigate. These depend on the signs of  $\kappa_\gamma$  and  $\kappa_a$ : (i) For  $\kappa_\gamma > 0$  and  $\kappa_a < 0$  no radiation occurs. (ii) For  $\kappa_\gamma > 0$  and  $\kappa_a > 0$  vacuum Čerenkov radiation may occur when the charged particle's speed exceeds 1, the low energy speed of light. We call this Type I VČR. (iii) For  $\kappa_\gamma < \kappa_a$  vacuum Čerenkov radiation occurs either when the charged particle's speed exceeds the low energy speed of light or when it exceeds the speed of the ultra-high energy photon. We call this last case Type II VČR. These cases show that VČR could occur in the first, fourth, and part of the third quadrants.

We present the threshold calculation first a charged particle  $a$ . In Section 4 we use these results for electrons and protons. The threshold calculations can be found using the methods use employed above or, equivalently, using the Čerenkov condition  $v_a > v_\gamma$ . Using the later method we find that for high energy charged particles the condition for Type I VČR is

$$p_{a_*} = \left[ \frac{m_a^2}{2\ell_p \kappa_a} \right]^{1/3} \quad \text{for } \kappa_a > 0. \quad (17)$$

This condition corresponds to the momentum at which the particle's speed exceeds 1, the low energy speed of light. This process the photon emission begins with long wavelength photons. For this Type I radiation the spectrum extends from zero energy up to  $p_{\gamma_{max}} = p_{a*}$ .

When  $\kappa_\gamma < \kappa_a$ , however, the emission process starts with finite energy photons. For high energy particles and photons – what we call Type II VČR – the Čerenkov condition yields

$$p_{a*} = \left[ \frac{m_a^2}{2(\kappa_a - \kappa_\gamma)\ell_p} \right]^{1/3} \quad \text{for } \kappa_a > \kappa_\gamma. \quad (18)$$

This may also be derived using the methods of Section 3.2. The observational constraints may be derived from this threshold.

When using the velocity relation, one must also ensure that energy is conserved. We study the case in which both outgoing particles have high momenta. In the leading order approximation of Eq. (4), the energy-momentum constraint takes on the familiar form of the threshold calculations:

$$\frac{m_a^2}{p_a} + \kappa_a \ell_p p_a^2 = \frac{m_a^2}{(p_a - p_\gamma)} + \kappa_a \ell_p (p_a - p_\gamma)^2 + \kappa_\gamma \ell_p p_\gamma^2.$$

After some simplification, this gives a quadratic for  $p_\gamma$

$$p_\gamma^2 - \frac{(3\kappa_a + \kappa_\gamma)p_a}{(\kappa_a + \kappa_\gamma)} p_\gamma - \frac{m_a^2 - 2\kappa_a \ell_p p_a^3}{(\kappa_a + \kappa_\gamma)\ell_p p_a} = 0. \quad (19)$$

The requirements that the physical root of this equation,  $p_{\gamma*}$ , be real and positive produce the threshold value

$$p_{a*} = \left[ \frac{-4m_a^2(\kappa_a + \kappa_\gamma)}{(\kappa_a - \kappa_\gamma)^2 \ell_p} \right]^{1/3} \quad \text{for } \kappa_\gamma < -3\kappa_e < 0. \quad (20)$$

The last inequality arises from the positivity of the maximum energy outgoing photon

$$p_{\gamma*} = \frac{(3\kappa_a + \kappa_\gamma)}{2(\kappa_a + \kappa_\gamma)} p_{a*}. \quad (21)$$

The two types of VČR have distinct spectra. For Type I, the emission of photons starts with very low energy photons and extends up to the particle's energy  $p_{\gamma_{max}} = p_a$ . For Type II VČR, the spectrum forms a band which begins at the finite energy corresponding to the condition  $v_a(p) = c_\gamma(p)$  and extends up to the particle's energy  $p_a$ . The half angles of the Čerenkov cone apertures also differ for the two types of radiation. The angle may be simply computed from Eq. (16). For Type II,

$$\theta_C \approx \left[ \frac{m_a^2}{p_a^2} (1 - \kappa_\gamma \ell_p p_\gamma) - 2\kappa_a \ell_p p_a \right]^{1/2}. \quad (22)$$

The angle for Type I is found by setting  $\kappa_\gamma = 0$  in the above equation.

Using observations of high energy electrons and protons, we can establish limits on the possible values of  $\kappa_e$  and  $\kappa_p$ . This is done in the final section.

**3.6. Proton Non-Absorption:**  $p + \gamma \not\rightarrow p + \pi^0$ . Shortly after the cosmic microwave background was discovered, Greisen [20] and Zatsepin and Kuzmin [21] predicted that the cosmic ray spectrum should have a cutoff. They found that cosmic rays constituents including protons and some heavier nuclei arriving from cosmological distances would lose energy through interactions with the CMB photons. The dominant process, photopion production, provides an effective energy cutoff for high energy protons from cosmological sources. In fact the spectrum was believed to be bounded from above by  $5 \times 10^{19}$  eV. However, the observed spectrum extends well above this cutoff to  $3 \times 10^{20}$  eV. While the number of events with energies above the GZK cutoff is not large ( $\sim 20$ ), the locations on the sky are not inconsistent with the hypothesis that the sources are isotropic. If these events are indeed particles originating from cosmological distances then the GZK cutoff must be modified. As observed in [5], the modified dispersion relations considered here can raise the GZK cutoff.

The method for computing the threshold energy for photopion production is similar to the above process but the details make the problem more complex. The different masses of the pion and the proton mean that much of the simplifications used above do not work. This returns us to the general two-channel case and the resulting quintic for the momentum  $p_c$ . In addition, when  $\kappa_p$  is negative, large asymmetries are favored. In fact, the threshold process produces a low momentum pion which means that we must use the dispersion relations of Eq. (3) instead of the leading order approximation. Hence the constraint on  $\kappa_p$  was found numerically.

Using threshold values in the range  $1 \times 10^{19}$  -  $8 \times 10^{20}$  eV we performed a search for the value of  $\kappa_p$  which separated the parameter space into a region in which the high energy proton would be stable and a region where it would be unstable. The selection criteria were simply that  $E_p + \epsilon > E'_p + E_\pi$ , where the energies are expressed using the modified dispersion relations of Eq. (3), and  $\epsilon$  is the energy of the cosmic microwave background photon,  $7 \times 10^{-4}$  eV. Conservation of 3-momentum was also required. Since the  $\kappa$  parameters for both pion and proton are identical, the procedure produced a constraint on  $\kappa_p$  as a function of proton threshold energy.

This function has the familiar shape of the effective potential of a particle in a central potential. At energies below the GZK cutoff  $\kappa_p$  is positive, effectively lowering the threshold. At the GZK cutoff  $\kappa_p$  passes through zero. However, the dependence of  $\kappa_p$  on the threshold energy is not a monotonically decreasing function. To see this note that since the magnitude of the proton correction term is larger than the magnitude of the correction terms of the products, at energies above the GZK cutoff  $\kappa_p$  must be negative. At significantly higher energies  $\kappa_p$  approaches zero from below (as may also be seen with energy-momentum conservation in the leading order approximation). The resulting function has a minimum of  $-7.9 \times 10^{-16}$  at  $1.6 \times 10^{20}$  eV. Thus, measurements of higher energy cosmic rays will not restrict the parameter further. These results are discussed further in the next section.

#### 4. LIMITS ON $\kappa$ -PARAMETERS

With all the above processes, one can derive limits on the modifications to the dispersion relations. The threshold constraints of Section 3 determine the allowed regions in the  $\kappa_e - \kappa_\gamma$  and  $\kappa_p - \kappa_\gamma$  parameter spaces. These constraints are summarized in Table 1. With the threshold energies in hand one can plot the constraints

Process Type	Constraint	Applicability
<i>Photon Stability</i> ( $\gamma \not\rightarrow e^- + e^+$ )		
Symmetric momenta	$\kappa_\gamma < \frac{1}{2}\kappa_e + \frac{4m_e^2}{\ell_p p_{\gamma_5}^3}$	$\kappa_\gamma \geq 0$
Asymmetric momenta	$(\kappa_\gamma - \kappa_e)^2 + \frac{8m_e^2 \kappa_e}{p_{\gamma_*}^3 \ell_p} < 0$	$\kappa_e < \kappa_\gamma < 0$
<i>Photon non-absorption</i> ( $\gamma + \gamma_{IR} \not\rightarrow e^- + e^+$ )		
Symmetric momenta	$2\kappa_\gamma + \frac{8\epsilon}{\ell_p p_{\gamma_*}^2} - \kappa_e - \frac{8m_e^2}{\ell_p p_{\gamma_*}^3} < 0$	$\kappa_\gamma > -\frac{4\epsilon}{\ell_p p_{\gamma_*}}$
Asymmetric momenta	$(\kappa_\gamma + \frac{4\epsilon}{\ell_p p_{\gamma_*}^2} - \kappa_e)^2 + \frac{8m_e^2 \kappa_e}{p_{\gamma_*}^3 \ell_p} < 0$	$\kappa_\gamma < -\frac{4\epsilon}{\ell_p p_{\gamma_*}}$
<i>Pion Stability</i> ( $\pi \not\rightarrow \gamma + \gamma$ )		
Symmetric momenta	$\kappa_\gamma < 2\kappa_\pi + \frac{2m_\pi^2}{\ell_p p_{\pi_*}^3}$	$\kappa_\gamma > 2\kappa_\pi$ and $\kappa_\gamma > 0$
Asymmetric momenta	$\kappa_\gamma < \kappa_\pi + \frac{m_\pi^2}{\ell_p p_{\pi_*}^3}$	$\kappa_\gamma > \kappa_\pi$ and $\kappa_\gamma < 0$
<i>Proton Stability</i> ( $p + \epsilon \not\rightarrow p + \pi$ )		
Numerical Result	$\kappa_p < -8 \times 10^{-16}$	
<i>Vacuum Čerenkov Radiation</i> ( $a \not\rightarrow a + \gamma$ )		
Type I: Zero-energy photon	$\kappa_a < \frac{m_a^2}{2\ell_p p_{a_*}^3}$	$\kappa_\gamma > 0$ or $\kappa_e > 0$
Type II: Finite-energy photon	$\kappa_\gamma > \kappa_a - \frac{m_a^2}{2\ell_p p_{a_*}^3}$	$\kappa_\gamma < 0$
Energy Conservation	$(\kappa_a - \kappa_\gamma)^2 + \frac{4m_a^2}{\ell_p p_{a_*}^3} (\kappa_a + \kappa_\gamma) < 0$	$\kappa_\gamma < 0, \kappa_\gamma < \kappa_a, \kappa_\gamma < -3\kappa_a$

TABLE 1. Summary of constraints and their regions of applicability.

and determine the allowed regions. But before discussing these plots, we summarize the observational data which provide threshold values for each of the processes.

We already discussed in Section 3.2 the observation which we use for photon stability (the 50 TeV event from the Crab nebula). We now turn to photon non-absorption by the far infra red background.

The unexpected transparency of the universe for high energy photons may be due Lorentz symmetry corrections (see, however, Ref. [45]). Although direct measurements from two instruments onboard COBE and detailed calculations have been completed, the IR flux is not well-determined [46]. This is largely due to, on the observational side, the flux of IR radiation produced by interplanetary dust and, on the calculational side, uncertainties in the galactic-evolution models. Given the uncertainties in the IR flux, we only plot an example case. The photon non-absorption constraint has a complex dependence on energy. Nonetheless, in the relevant region

the threshold energy which allows for the maximum increase in transparency due to suppressed pair creation induced by background 0.025 eV IR photons is 15 TeV. In the summary plots we use this energy as a representative case. If the unexpected transparency is due to Lorentz symmetry corrections then this constraint is the lower boundary on the allowed region.

At shorter wavelengths the spectrum is much better established. In fact, with no modifications the universe becomes highly opaque to photons above  $\sim 100$  TeV from the interactions with the 2.7K cosmic background radiation [46]. Observations of photons above this “hard limit” would necessitate more serious consideration of photon non-absorption due to modifications to Lorentz symmetry.

As shown in Section 3.4 modified dispersion relations can make the pion stable (see also [4, 19]). Recently Antonov *et. al.* reported on a test of Lorentz invariance using longitudinal development of extensive cosmic air showers [27]. They found that simulated air showers produced a better fit to the observed depth of the highest energy air shower [22] if the pion became stable at high energies. This stability could be achieved if pions are stable above  $p_{\pi^*} \sim 10^{18}$  eV. We use this threshold value in the  $\kappa_p - \kappa_\gamma$  plot. This becomes a very restrictive limit.

Vacuum Čerenkov radiation provides a strong restriction “from the bottom” in  $\kappa_a - \kappa_\gamma$  parameter space. We consider limits on the allowed region in the parameter space for both electrons and protons. The limit for electrons comes from observations of a supernova remnant. The best fit for the X-ray spectrum from the supernova remnant SN 1006 arises from assuming that the radiation is synchrotron radiation from electrons with energies up to  $\sim 100$  TeV [47, 48]. The highest energy primary cosmic rays are believed to be protons [27]. As we see next the cosmic ray spectrum reaches  $3 \times 10^{20}$  eV. We use this limit for VČR for protons.

Finally, cosmic rays above the GZK cutoff are observed. This cutoff may be raised by modified dispersion relations. Using the highest observed cosmic ray,  $3 \times 10^{20}$  eV for the threshold, we would obtain the constraint  $\kappa_p < -5.6 \times 10^{-16}$ . There are two interesting features to this result. First, there is minimum at  $1.6 \times 10^{20}$  eV in the  $\kappa_p$ -energy curve discussed in Section 3.6. To prevent a gap in the cosmic ray spectrum between  $1.1 \times 10^{20}$  and  $3 \times 10^{20}$  eV we use the value of  $\kappa_p$  at the minimum,  $-8 \times 10^{-16}$ . Second, even when one accounts for the uncertainties reported in Ref. [22] the constraint is not consistent with  $\kappa_p = 0$ . Attributing the raising of the GZK threshold modifications of the dispersion relations restricts the hadronic parameter to negative values and effectively rules out exact Lorentz invariance.

In Figures (2) and (3) we identify the allowed regions of  $\kappa_e - \kappa_\gamma$  and  $\kappa_p - \kappa_\gamma$  parameter space. We include all the above processes, including the more speculative processes of the photon non-absorption, proton non-absorption, and pion stability. This allows us to check whether a consistent set of parameters exist which simultaneously explain the three paradoxes mentioned in the introduction and are consistent with current observations.

In the electron-photon plot of Figure 2 we include constraints from photon stability, vacuum Čerenkov radiation, and photon non-absorption. The allowed region is a tightly constrained area mostly lying in the third quadrant and containing the origin. Thus, based on these processes it appears that quantum geometry effects reduce the energy (and speed) of particles at high momentum. As Fig. (2b) reveals, however, there is a region in which positive values of the parameters are allowed. The allowed region contains the origin and a tiny sliver of positive  $\kappa_e$  corresponding

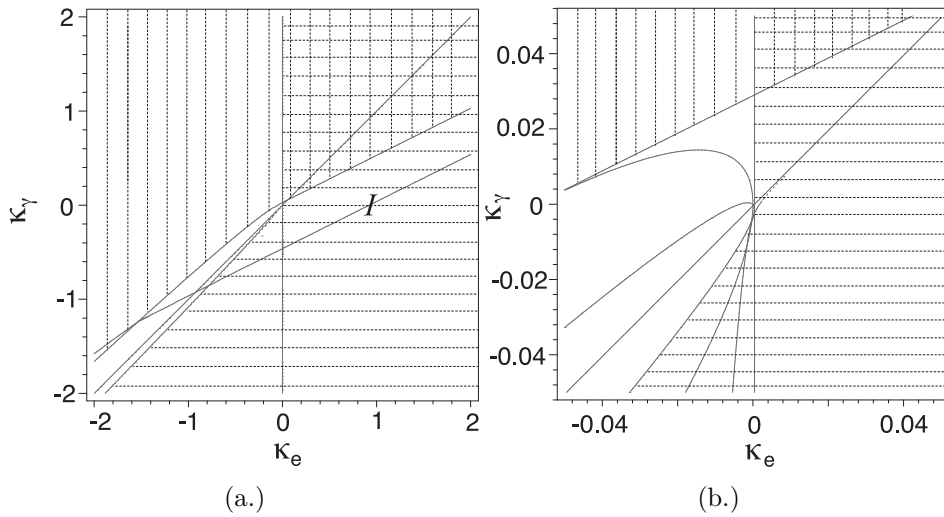


FIGURE 2. Plots of the allowed regions in  $\kappa_\gamma - \kappa_e$  parameter space. The unshaded portion shows the region in which corrections to Lorentz invariance are consistent with current observational limits. In (a) limits from photon stability, vacuum Čerenkov radiation, and photon non-absorption are shown. The vertical shading corresponds to the photon stability constraint while the horizontal shading corresponds to vacuum Čerenkov radiation. The constraint labeled  $I$  arises from assuming that high energy photons are not absorbed in pair creation. If so, this provides a lower limit on the allowed region. In (b) the same constraints are shown in a region around the origin. The shading is the same as in (a).

to superluminal electrons ( $\kappa_e < 4.5 \times 10^{-4}$ ). The  $\kappa_\gamma$  parameter is not as tightly confined around the origin and is less than  $\sim 0.03$ .

In the hadron-photon plot of Figure 3 the limits are obtained from the processes pion stability, proton non-absorption, and vacuum Čerenkov radiation. The quadratic VČR constraints do not show up on this scale due to the high upper limit on proton energy,  $3 \times 10^{20}$  eV. In this plot the allowed region is an exceedingly narrow band again mostly in the third quadrant; the scale is on the order  $10^{-10}$ . There is a small region of positive values of the parameters allowed. The band of allowed values is constrained by the pion stability from above and VČR from below.

If these two constraints are borne out by further observations, different modifications of Lorentz invariance of this form for hadronic and massless particles would be effectively ruled out. It is also interesting that the case  $\kappa_p = \kappa_\gamma$  lies nearly on the boundary of the allowed region. The difference of this relation and the VČR constraint is  $\sim 10^{-15}$ .

We also note that the allowed region does *not* contain  $\kappa_p = 0$ , the Lorentz symmetric case. This is due to the raising of the GZK threshold. It is likely that the GZK threshold may be explained by other means. Nonetheless, if the GZK cutoff is raised by corrections of this form, then current observations rule out exact Lorentz symmetry. So if we take the three conditions of pion stability,

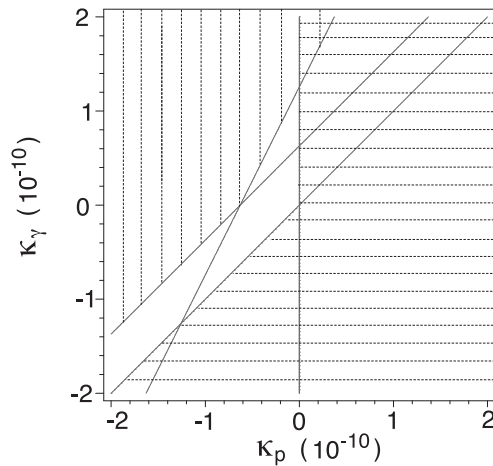


FIGURE 3. The plot of the allowed region in the  $\kappa_\gamma - \kappa_p$  space. Constraints arising from pion stability, proton non-absorption, and vacuum Čerenkov radiation are shown. The vertical shading is due to the pion stability constraint while the horizontal shading comes from VČR. The constraints due to proton non-absorption and VČR appear to be a single vertical line.

proton non-absorption, and VČR seriously, then the Lorentz symmetry is broken and the parameters are extremely finely tuned to each other. From the plot and the constraints on  $\kappa$  from the semiclassical analysis, we conclude that  $\kappa_p = \kappa_\gamma \neq 0$ .

Finally, it is also clear that nearly all the positive  $\kappa$  space is ruled out. In particular, the results for massive particles effectively rule out “faster than light” behavior. One reason why this is significant is that satisfies the classical notion of causality thereby satisfying one of the requirements for consistency in perturbative quantum field theory.

It is important to keep in mind that these are preliminary results. Our strategy is to combine all processes to see whether the results are consistent. But it is clear that these constraints are not equally precise. For instance the vacuum Čerenkov radiation constraints are tentative. The limits for electrons are derived from indirect measurements of synchrotron radiation around a single supernova remnant. We need more data on high energy electrons and cosmic rays before these processes can truly rule out regions of the parameter space.

Our VČR limit for hadrons could also be called “soft.” We assume that the highest energy cosmic ray event was due to a proton. As new cosmic ray data becomes available we will be able to better judge the validity of this assumption. Once the Pierre Auger project [49] is running we should have a much better idea of the value of the threshold. Aside from data from more ultra-high energy events, this detector should also determine the mass composition of the primary cosmic rays. This is absolutely critical for the study of Lorentz symmetry modifications.

Much better estimates of the far infra red background are needed before we can establish the lower limit of the allowed region in  $\kappa_e - \kappa_\gamma$  parameter space. Without this bound we can not confine the parameters to a finite area. In Ref. [13] the

uncertainty is the background is handled in a different way. Assuming that the actual threshold lies between 10 TeV and 20 TeV they confine the allowed area to a finite size.

The pion stability constraint will also be improved with new cosmic ray data. The results of Ref. [27] compare simulated showers with the single, highest energy cosmic ray event [22]. It will be very interesting to see whether the onset of pion stability is observed in other ultra-high energy showers.

The only constraint which could be considered a hard limit comes from photon stability. This sharply restricts the possible superluminal behavior of ultra-high energy photons. As higher energy gammas are observed from local sources, this constraint will “push down” on the allowed region.

## 5. CONCLUSIONS

Beginning with a form of modified dispersion relations, we use exact energy-momentum conservation, to derive thresholds for particle processes. The dispersion relations we consider are motivated by a class of semiclassical states of loop quantum gravity which are classical and flat above a characteristic length scale [16, 17]. We work in a model in which there are separate parameters for modifications of the dispersion relations for photons, leptons, and hadrons. The process thresholds provide a sensitive test of the quantum geometry effects. In some cases, such a photon decay and vacuum Čerenkov radiation, normally forbidden processes are activated at high energy. In other cases, such a pion decay, processes are suppressed.

Current TeV-scale observations offer severe restrictions on the nature of these effects. There exist allowed regions in both parameter spaces consistent with all of the above processes. The results are summarized in Figures 2 and 3 and in the last section. In particular, including all of the processes the analysis shows that the hadronic parameter is effectively equal to the photon parameter and both of these are non-zero. Further the lepton parameter is confined to a band in the third quadrant as shown in Fig. 2.

**Acknowledgment.** *We thank members of the Hamilton College Department of Physics, the Perimeter Institute, Hugo Morales-Técolt, and David Mattingly for helpful discussions during this work. T.K. was supported, in part, by the Ralph E. Hansmann Science Students Support Fund of Hamilton College.*

## REFERENCES

- [1] C. Rovelli, “Loop Quantum Gravity” *Living Reviews in Relativity* at <http://www.livingreviews.org/Articles/Volume1/1998-1rovelli> and M. Gaul and C. Rovelli, “Loop Quantum Gravity and the Meaning of Diffeomorphism Invariance” *Lect. Notes Phys.* **541** (2000) 277-324; gr-qc/9910079.
- [2] V. A. Kostelecky and S. Samuel, *Phys. Rev.* **D 39** (1989) 683.
- [3] G. Amelino-Camilia et. al., *Nature* **393** (1998) 763.
- [4] S. Coleman and S. L. Glashow, *Phys. Rev.* **D 59** (1999) 116008.
- [5] T. Kifune, *Astrophys. J* **518** (1999) L21.
- [6] W. Kluzniak, *Astropart. Phys.* **11** (1999) 117.
- [7] O. Bertolami and C.S. Carvalho, *Phys. Rev.* **D 61** (2000) 103002.
- [8] J. Ellis, N.E. Mavromatos, D.V. Nanopoulos, “ Probing Models of Quantum Space-Time Foam” gr-qc/9909085.
- [9] R. Aloisio et. al., *Phys. Rev.* **D 62** (2000) 053010.
- [10] G. Amelino-Camilia and T. Piran, *Phys. Rev.* **D 64** (2001) 036005.
- [11] F. W. Stecker and S. L. Glashow, *Astropart. Phys.* **16** (2001) 97.



- [12] J. Ellis, N.E. Mavromatos, D.V. Nanopoulos, “Space-Time Foam Effects on Particle Interactions and the GZK Cutoff” *Phys. Rev. D* **63** (2001) 124025; hep-th/0012216.
- [13] T. Jacobson, S. Liberati, D. Mattingly, “TeV Astrophysics Constraints on Planck Scale Lorentz Violation” hep-ph/0112207. See also “High Energy Constraints on Lorentz Symmetry Violations” hep-ph/0110094.
- [14] J. Alfaro and G. Palma *Phys. Rev. D* **65** (2002) 103516.
- [15] R. Gambini and J. Pullin, *Phys. Rev. D* **59** (1999) 124021.
- [16] J. Alfaro, H. A. Morales-Técotl, L. F. Urrutia, “Quantum Gravity Corrections to Neutrino Propagation” *Phys. Rev. Lett.* **84** 2318; gr-qc/9909079.
- [17] J. Alfaro, H. A. Morales-Técotl, L. F. Urrutia, “Loop Quantum Gravity and Light Propagation” *Phys. Rev. D* **65** (2002) 103509; hep-th/0108061.
- [18] N. R. Bruno, G. Amelino-Camelia, J. Kowalski-Glikman, *Phys. Lett. B* **522** (2001) 133.
- [19] G. Amelino-Camelia, “Space-time quantum solves three experimental paradoxes” gr-qc/0107086.
- [20] K. Greisen, *Phys. Rev. Lett.* **16**, 748 (1966).
- [21] G. T. Zatsepin and V. A. Kuzmin, *JETP Lett.* **41** (1966) 78.
- [22] D. J. Bird et. al., *Astrophys. J.* **424** (1994) 491.
- [23] M. Takeda et. al., *Phys. Rev. Lett.* **81** (1998) 1163.
- [24] R. J. Protheroe and H. Meyer, *Phys. Lett. B* **493** (2000) 1-6.
- [25] F. Krennrich et. al., astro-ph/0107113.
- [26] F.A. Aharonian, *Astron. Astrophys.* **349** (1999) 11A.
- [27] E. E. Antonov et. al., *JETP Lett.* **73** (2001) 446.
- [28] H. A. Morales-Técotl, *private communication*.
- [29] M. Varadarajan and J. Zapata, “A proposal for analyzing the classical limit of kinematic loop gravity” *Class. Quant. Grav.* **17** (2000) 4085-4109.
- [30] T. Thiemann, *Class. Quant. Grav.* **18** (2001) 2025.
- [31] T. Thiemann and O. Winkler, *Class. Quant. Grav.* **18** (2001) 2561-2636, 4629-4682, and 4997-5054.
- [32] H. Sahlmann, T. Thiemann, O. Winkler, *Nucl. Phys. B* **606** (2001) 401-440.
- [33] A. Corichi and J. Reyes, “A Gaussian Weave for Kinematical Loop Quantum Gravity” *Int. J. Mod. Phys. D* **10** (2001) 325-338.
- [34] M. Varadarajan, “Photons from quantized electric flux representations” *Phys. Rev. D* **64** (2001) 104003.
- [35] A. Ashtekar and J. Lewandowski, “Relation between polymer and Fock excitations” *Class. Quant. Grav.* **18** (2001) L117-L128.
- [36] R. Gleiser and C. Kozameh, “Astrophysical limits on quantum gravity motivated birefringence” *Phys. Rev. D* **64** (2001) 083007.
- [37] Bear et. al., *Phys. Rev. Lett.* **85** (2000) 5038.
- [38] Berglund et. al., *Phys. Rev. Lett.* **75** (1995) 1879.
- [39] J. Kowalski-Glikman and S. Nowak, hep-th/0203040.
- [40] G. Amelino-Camelia, *Phys. Lett. B* **510** (2001) 255-263, *Int. J. Mod. Phys. D* **11** (2002) 35-60.
- [41] J. Maguejo and L. Smolin, “Lorentz invariance with an invariant energy scale” hep-th/0112090.
- [42] V. Kostelecky and R. Lehnert, “Stability, causality, and Lorentz and CPT violation” *Phys. Rev. D* **63** (2001) 065008.
- [43] T. Tanimori et. al., *Astrophys. J.* **492** (1998) L33.
- [44] T. Konopka, “Possible Effects of Quantum Gravity on Ultra High Energy Particles” *BA Thesis* Hamilton College 2001.
- [45] O.C. de Jager and F.W. Stecker, *Astrophys. J.* **566** (2002) 738; astro-ph/0107103.
- [46] V. Berezhinsky, “Puzzles in Astrophysics in the Past and Present” astro-ph/0107306.
- [47] S. Reynolds, “Synchrotron Models for X-rays from the Supernova Remnant SN 1006” *Astrophys. J.* **459** (1996) L13.
- [48] K. Koyama et. al., *Nature* **378** (1995) 255.
- [49] See The Pierre Auger Project [www.auger.org](http://www.auger.org).